

# Minority carrier lifetime and iron concentration measurements on *p*-Si wafers by infrared photothermal radiometry and microwave photoconductance decay

M. E. Rodríguez,<sup>a)</sup> A. Mandelis, G. Pan, and J. A. García

*Photothermal and Optoelectronic Diagnostics Laboratories (PODL), Department of Mechanical and Industrial Engineering, University of Toronto; and Materials and Manufacturing Ontario, 5 King's College Road, Toronto, Ontario, M5S 3G8, Canada*

V. Gorodokin and Y. Raskin

*Sizary Ltd., Tefen Industrial Park, Building 4A, Migdal Tefen 24959, Israel*

(Received 24 September 1999; accepted for publication 6 March 2000)

A comparative study of electronic transport properties of *p*-Si wafers intentionally contaminated with Fe was performed using infrared photothermal radiometry (PTR) and microwave photoconductance decay ( $\mu$ -PCD). Strong correlations were found between PTR and  $\mu$ -PCD lifetimes in a lightly contaminated wafer with no significant PTR transient behavior. The absolute PTR lifetime values were larger than the local averaged  $\mu$ -PCD values, due to the different excitation wavelengths and probe depths. In a heavily contaminated wafer the  $\mu$ -PCD and PTR lifetime correlation was poorer. PTR measurements were highly sensitive to iron concentration, most likely due to the dependence of the bulk recombination lifetime on it. Rapid-scanned (nonsteady-state) PTR images of the wafer surface exhibited strong correlations with both  $\mu$ -PCD lifetime and [Fe] concentration images in both heavily and lightly contaminated wafers. For the lightly and uniformly contaminated wafer, PTR scanning imaging was found to be more sensitive to iron concentration and lifetime variations than  $\mu$ -PCD images. © 2000 American Institute of Physics. [S0021-8979(00)08111-1]

## I. INTRODUCTION

The physical and electronic properties of semiconductor wafers directly affect the performance of various devices fabricated on these wafers. In recent years, the evaluation of semiconductors by means of photothermal methods has attracted particular attention, owing to the nondestructive and noncontact character of these techniques. Photothermal radiometry (PTR)<sup>1,2</sup> has been shown to possess distinct advantages, such as remote *in situ* evaluation and optimal sensitivity to the electronic transport properties of the laser photoexcited material.<sup>3</sup> Using the three-dimensional (3D)-PTR technique<sup>4,5</sup> due to spatial constraints imposed by tightly focused Gaussian laser beams, one can obtain electronic transport parameters of Si wafers, including the carrier recombination lifetime,  $\tau$ , the minority carrier diffusion coefficient,  $D_n$ , or  $D_p$ , the carrier diffusion length,  $L_D$ , the front surface recombination velocity,  $S_1$ , as well as the thermal diffusivity,  $\alpha$ .

Physically, the signal generation process can be described as follows. Upon impinging on a semiconductor surface, an intensity-modulated laser beam simultaneously produces direct lattice heating due to absorption, as well as a modulation in the free photoexcited carrier density, provided the photon energy is greater than the band gap energy. The

modulated photoexcited free-carrier density depends on the laser fluence and on the electronic properties of the material in the vicinity of the laser beam. If a wide-bandwidth infrared (IR) detector, such as mercury-cadmium-telluride (HgCdTe, MCT; Fig. 1), is focused on a laser photoexcited spot of the sample, a *superposition* of IR radiative emissions from the excited region may be measured. Unlike conventional photoluminescence, this IR radiation is mainly due to the optical deexcitation of photoexcited carriers, with the simultaneous emission of an infrared photon within the black-body (Planck) spectral range.<sup>2</sup> In other words, each deexciting carrier acts like a Planck radiator. The collected signal is the vector sum of this depth-integrated radiation, diffusely emitted by the photogenerated free-carrier plasma-wave density, plus the conventional modulated IR radiation (thermal wave), generated by direct heating due to lattice absorption of the incident laser radiation, and by delayed recombination lifetime-controlled heating due to nonradiative deexcitations of carriers.<sup>2</sup> The signal dependence on the depth integral of the carrier density provides an important diagnostic mechanism for PTR, which thus carries information on carrier diffusion and recombination mechanisms. In typical-quality industrial Si wafers it turns out that the major advantage of PTR over other photothermal methods, including the commercially widely used photomodulated thermoreflectance (PMOR) technique,<sup>6</sup> is the almost complete domination over the thermal-wave response of the signal by the electronic plasma-wave component at all modulation frequencies (Hz to MHz).<sup>3</sup> Therefore, PTR appears to be ideally suitable as a

<sup>a)</sup> Author to whom correspondence should be addressed; on leave from: Centro de Investigación en Ciencia Aplicada y Tecnología Avanzada del I.P.N., Unidad Queretaro, Jose Siurob 10 Col. Alamedas, Queretaro México; electronic mail: mario@mie.utoronto.ca

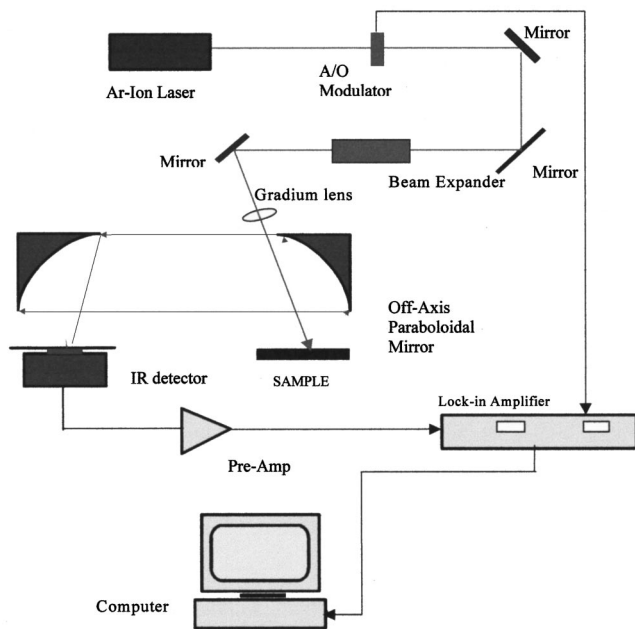


FIG. 1. Experimental PTR arrangement for Si wafer inspection and lifetime imaging.

diagnostic technology in assessing the electronic quality of semiconductor substrates and processed wafers.

Another technique widely used for evaluation of lifetime and impurity monitoring of semiconductors, which depends on the depth integral of photoexcited free-carrier densities is microwave photoconductance decay ( $\mu$ -PCD).<sup>7-10</sup> In this technique an excess electron-hole pair concentration is created by optical-laser illumination. The photocurrent (PC) signal is proportional to the number of excess electron-hole pairs integrated over the entire wafer volume. The PC decay is monitored by the change in microwave power reflected from the sample. The carrier transport problem is considered to be *one dimensional* since the laser spot size is much larger than either the wafer thickness or the carrier diffusion length.<sup>9</sup> Microwaves are not only reflected from the surface, but also they penetrate approximately one skin depth into the sample. Typical skin depths in Si at 10 GHz lie between 350  $\mu\text{m}$  for  $\rho=0.5 \Omega \text{ cm}$  and 2200  $\mu\text{m}$  for  $\rho=10 \Omega \text{ cm}$ . A good portion of the wafer can be sampled by microwaves and the microwave reflection signal is characteristic of the *deep bulk* carrier density. The lowest value of minority recombination lifetime ( $\tau$ ) that can be determined depends on wafer resistivity. Different measurement methods can give widely differing values of carrier lifetimes for the same material or device structure. In most cases, the reasons for these discrepancies are fundamental and are not due to a deficiency of the measurement. The difficulty with defining a lifetime is that we are describing localized properties of a carrier within the semiconductor rather than the properties of the semiconductor itself.<sup>11</sup> Usually a single numerical value of lifetime is given, but this value is directly related to other parameters, such as surface states at front and back interfaces, doping barriers, and density of carriers, besides the properties of the semiconductor substrate material and its temperature.

It is well known that wafer contamination by fast diffusing metals like Fe is a yield-reducing factor in integrated circuits. Iron detection in  $\text{B}^+$ -doped  $p$ -Si depends on the behavior of FeB complexes in different states. Following FeB dissociation, the concentration of iron interstitial ( $\text{Fe}_i$ ) can be influenced by temperature or optical activation. Since Fe acts as a more effective recombination center in Si than FeB does, the difference in measured effective lifetime before and after breaking FeB pairs can be used for the qualitative determination of defect concentration maps related to iron. In this work, this method has been used to measure  $\mu$ -PCD lifetimes before and after Fe-B dissociation and to extract  $[\text{Fe}]$  concentrations.<sup>7,8,12-14</sup> The lifetime/iron concentration dependence is strong for  $p$ -Si with Fe in interstitial states and much less so for Fe as FeB complex. For low injection levels the lifetime in the activated  $\text{Fe}_i$  state is smaller than in the FeB complex.<sup>7,8</sup>

In this article we describe the first PTR characterization of Fe-contaminated  $p$ -Si wafers and the calculation of several carrier transport parameters by means of a 3D PTR model.<sup>4,5</sup> In addition, PTR-derived parameters have been compared with similar measurements using the  $\mu$ -PCD technique. The latter was chosen because the signal generation process is quite similar between these two techniques. The first qualitative and quantitative comparison of PTR and  $\mu$ -PCD carrier recombination lifetimes and scanned images of nonuniformly (heavily) and uniformly (lightly) Fe contaminated Si wafers is presented and conclusions are drawn as to the sensitivity of PTR images to  $[\text{Fe}]$  contamination distribution and its effect on recombination lifetimes.

## II. PTR EXPERIMENTAL SETUP

The experimental setup for 3D PTR instrument for Si wafer diagnostics is shown in Fig. 1 and has been described in detail elsewhere.<sup>1,4,5</sup> An argon-ion laser beam (514.5 nm) is passed through an acousto-optic modulator (AOM) and a beam expander ( $10\times$ ) producing a 1 cm beam size. The spot size of the focused Gaussian laser beam is approximately 48  $\mu\text{m}$  in diameter attained by use of a gradium glass lens with 12.4 cm focal distance. The IR emission was collected by two off-axis paraboloidal mirrors and was focused onto a liquid-nitrogen-cooled MCT IR detector with spectral response between 2 and 12  $\mu\text{m}$ . The output signal was preamplified and fed to a lock-in amplifier and was processed by a personal computer. The excitation beam was modulated from 10 Hz to 100 kHz via an AOM. All the experimental measurements were normalized by a wide-bandwidth instrumental transfer function.<sup>4</sup> In recent work we have shown that the amplitude scales linearly with the recombination lifetime in some ranges of parameters typical of Si wafers.<sup>5</sup> Therefore, an  $x$ - $y$  infrared-radiation-amplitude scan of a Si substrate (with or without grown oxide) when it is properly calibrated in units of  $\mu\text{s}$ , yields, in principle, a recombination lifetime image of the scanned region. Such a radiometric image has been called a “*thermoelectronic image*,” or “*thermoelectronic scan*.” PTR thermoelectronic amplitude and phase

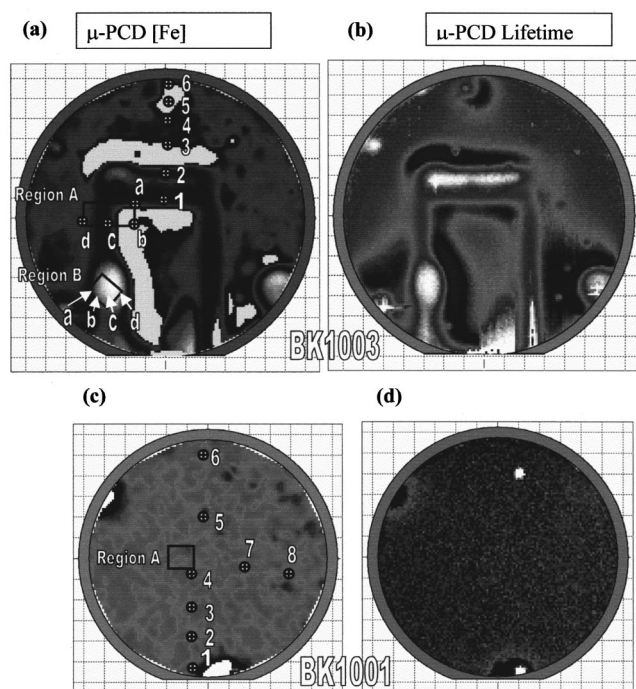


FIG. 2. The  $\mu$ -PCD [Fe] and  $\mu$ -PCD lifetime maps of samples BK1003 and BK1001, with schematic representation of locations and regions studied. Light-colored areas in Fig. 2(a) and 2(c) could not yield  $\mu$ -PCD lifetime information.

images were generated by moving two micrometer stages in the  $x$ - $y$  directions. The step used to build each image was 500  $\mu\text{m}$ .

### III. EXPERIMENTAL RESULTS AND DISCUSSION

Two  $p$ -type (boron-doped) Si wafers grown from magnetic Czochralski ingots, 5 and 6 in. in diameter (labeled BK1001 and BK1003, respectively), with resistivities between 10 and 20  $\Omega\text{ cm}$  and (100) crystallographic orientation, were investigated. The wafers were oxidized under standard oxygen flow (500  $\text{cm}^3/\text{min}$ ) in a mini furnace at 1000  $^\circ\text{C}$  for 70 min. and were inspected with a  $\mu$ -PCD probe after processing. Sample BK1001 was placed in a quartz boat vertically, while sample BK1003 was placed between two silicon carbide (SiC) boats horizontally. As a result, sample BK1001 received a relatively homogeneous Fe contamination of lower concentration than BK1003. This wafer was in contact with the SiC boats and thus received very inhomogeneous and heavier Fe contamination from both the solution and by contacting the boats.

The influence of Fe concentration on the thermoelectronic properties was studied in the low-injection regime (typically about 30 mW of optical power). These properties include minority recombination lifetime ( $\tau$ ), minority carrier diffusion coefficient ( $D_n$ ), front surface recombination velocity ( $S_1$ ), thermal diffusivity ( $\alpha$ ), and the plasma and thermal coefficients of the total PTR signal.<sup>3</sup> Figure 2 shows the  $\mu$ -PCD Fe concentration and lifetime maps of the entire wafer surface (BK1003, BK1001).<sup>7,8</sup> In sample BK1003 six radial points 1–6 and two regions were studied (1  $\text{cm} \times 2\text{ cm}$ , Region A; and 1  $\text{cm} \times 1\text{ cm}$ , Region B) [see Figs. 2(a) and

2(b)]. The  $\mu$ -PCD scans showed that sample BK1001 was much more uniform than sample BK1003 and was thus examined with PTR at eight locations along the radial direction as well as inside a small area [1  $\text{cm} \times 1\text{ cm}$ , Region A, Fig. 2(c)]. Unfortunately,  $\mu$ -PCD could not yield information about Fe concentration values inside the light regions across the sample BK1003, Fig. 2(a); and, to a much lesser extent, along the rims of BK1001, Fig. 2(c). The II-like shape in wafer BK1003 is the trace of a contact between the SiC boat pedestal and the Si wafer during the oxidation process and is a seat of heavy Fe contamination. The existence of PTR signal transients in these samples, a phenomenon exhibited by some wafers with electronically poor surfaces,<sup>15</sup> was observed, especially with BK1003. Therefore, frequency scans at each point used to calculate thermoelectronic properties were carried out only after steady-state signal conditions were established. Figure 3 shows the PTR signal for the six radial positions in sample BK1003. The theoretical fits are shown as continuous lines in that figure. Table I shows the thermal and electronic values associated with each spot as were obtained through a multi-parameter data fit of the 3D PTR theory.<sup>4,5</sup> The average local  $\mu$ -PCD carrier recombination lifetime values, extrapolated from the images in Fig. 2 with the help of calibration histograms (not shown) and the average [Fe] concentration, calculated for each spot in the same manner, are also given in Table I. It is seen that the lifetime trends between PTR and  $\mu$ -PCD measurements are well correlated, even though the PTR values are consistently higher. Recall that the PTR laser source wavelength was 514 nm, whereas  $\mu$ -PCD data were obtained with optical excitation at 904 nm. At this excitation wavelength, the optical absorption coefficient of Si is  $\beta = 1.1 \times 10^2\text{ cm}^{-1}$ , and the  $\mu$ -PCD skin depth is  $\lambda = 100\text{ }\mu\text{m}$ .<sup>16</sup> Both microwave and PTR detection for this wafer were effected from the front (polished) surface. Given the long excitation wavelength, the  $\mu$ -PCD optical probe “sees” deeper into the substrate and can be reasonably expected to yield shorter lifetime values from thoroughly Fe-contaminated wafers than the very-near-surface PTR probe. The measurements of PTR signals at the steady state may have also contributed to the differences found in the calculated lifetime values. The fact that many contaminated regions of our Si wafers exhibited moderate-to-strong transients under the PTR probe has forced the scanning imaging detailed below to be performed under early-time transient conditions, whereas transport property PTR measurements were made at the steady state. On the other hand,  $\mu$ -PCD measurements were essentially insensitive to the state of the surface. Therefore, it was not possible to construct meaningful linear  $\tau_{\text{PTR}}$  vs  $\tau_{\mu\text{-PCD}}$  calibration curves for samples that exhibit transients, since the two sets of parameters were obtained under very different conditions and the PTR signal is also sensitive to electronic surface states. For the three points (1,2,4), Fig. 2(a), where Fe concentration values were available, Table I shows a clear anti correlation between lifetime values and [Fe] as measured by  $\mu$ -PCD. Figure 4 consists of PTR lifetime and front-surface recombination velocity histograms, as functions of the radial direction at positions 1–6 of Fig. 2(a). According to these results, sample BK1003 generally exhibits roughly two distinct ra-

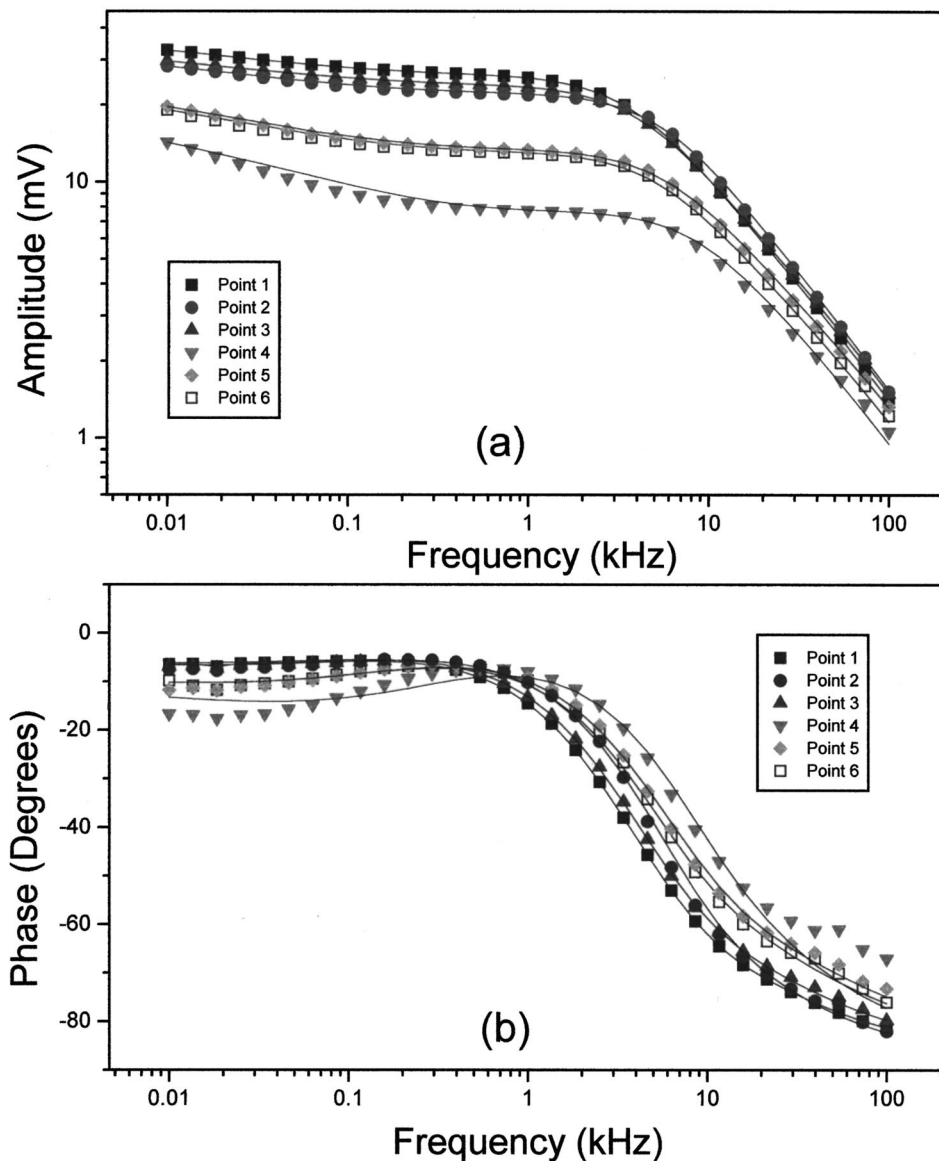


FIG. 3. PTR signal amplitude (a) and phase (b) for six points located on sample BK1003 [see Fig. 2(a)]. Continuous curves represent multi-parameter theoretical best fits to the data.

dial regions with different thermoelectronic characteristics: Region I (radius  $R < 3.8$  cm away from the center) with relatively long lifetimes; and Region II ( $3.8 < R < 5.9$  cm away from the center) with shorter lifetimes. Points located in Region II did not exhibit PTR transients, while points within the boundaries of Region I exhibited strong transient behavior. Furthermore, a clear anti correlation is seen between PTR  $\tau$  and  $S_1$  values across Regions I and II in Fig. 4. This trend has also been observed recently with regard to other oxidized Si wafers.<sup>5</sup> This anti correlation may be partly due to the very-near-surface probing of the 514 nm laser beam ( $\sim 1 \mu\text{m}$  optical absorption depth), which suggests that the measured value of  $\tau$  may be influenced by the electronic state of the surface (and thus the measured surface recombination velocity). It is concluded that further systematic work is needed to correlate the radial behavior of PTR lifetimes with wafer growth and processing history. In summary, the details of the PTR and  $\mu$ -PCD lifetime values appear to be affected by the local Fe concentration (Table I).

Figures 5(a) and 5(b) show the  $\mu$ -PCD lifetime and iron

concentration calibration histograms, respectively, for sample BK1003 after Fe activation, indicating a  $\tau$  range between 4 and 30  $\mu\text{s}$ . The  $\mu$ -PCD-determined Fe concentration in this sample varies from  $5 \times 10^9$  to  $3 \times 10^{12}$  atoms/cm<sup>3</sup>. The blowups in Figs. 5(c) and 5(d) show the lifetime and [Fe] maps of Region A (1 cm  $\times$  2 cm) located at the center of Fig. 2(a). Similar blowups in Figs. 5(e) and 5(f) show lifetime and [Fe] maps in Region B (1 cm  $\times$  1 cm) located in wafer BK1003.

In order to obtain a better understanding of the nature of PTR images in the presence of [Fe] concentration gradients across these Si wafer surfaces, Regions A and B in Fig. 2(a) were scanned at constant modulation frequency (1 kHz). Figure 6 shows PTR amplitude and phase images of Region A. This region was scanned using a 500  $\mu\text{m}$  step at a dwell time of 12 s step. As discussed above, due to the nonsteady nature of the PTR scan with contaminated wafers, all images of short dwell time compared to the saturation time of the signal must be regarded as transient.<sup>15</sup> Such images represent equitemporal slices after the onset of irradiation and only the

TABLE I. Steady-state thermal and electronic transport parameters of wafer BK1003 (6 in. diameter), determined from the 3-D PTR model, for six radial positions 1–6, and Region A and B, Fig. 2(a). The  $\mu$ -PCD lifetime and [Fe] concentration values are also shown.

Location from center (cm)	Amplitude (mV)	$\alpha$ (cm <sup>2</sup> /s)	$\tau_{PTR}$ ( $\mu$ s)	$D_n$ (cm <sup>2</sup> /s)	$S_1$ (cm/s)	Average $\tau_{\mu PCD}$ ( $\mu$ s)	Average [Fe](cm <sup>-3</sup> )
0.00 (1)	32.745	0.75	71	3.10	300	30	< 10 <sup>10</sup>
1.27 (2)	28.333	0.70	38	3.20	210	11	> 10 <sup>12</sup>
2.54 (3)	29.674	0.73	63	3.10	370	25–30	No data
3.81 (4)	14.275	0.65	26	5.00	850	19	5 × 10 <sup>11</sup>
5.08 (5)	19.707	0.70	45	4.60	750	25–30	No data
5.58 (6)	19.120	0.70	46	3.40	560	25–30	No data
Region A							
a	26.632	0.70	70	3.40	300	19	5 × 10 <sup>10</sup>
b	30.110	0.70	75	3.40	240	24	2 × 10 <sup>10</sup>
c	26.818	0.70	70	3.40	330	12	5 × 10 <sup>11</sup>
d	17.8681	0.50	35	3.40	280	18	6 × 10 <sup>10</sup>
Region B							
a	32.850	0.80	52	3.0	300	13	3 × 10 <sup>11</sup>
b	30.287	0.80	45	3.0	430	9	1 × 10 <sup>12</sup>
c	11.261	0.20	6	8.0	360	6	> 1 × 10 <sup>12</sup>
d	9.830	0.80	4	10.0	100	4	> 3 × 10 <sup>12</sup>

relative signal amplitudes and phases are meaningful with respect to all other signals obtained under the same conditions. Four points (a–d) located inside Region A, as indicated in Figs. 2(a) and 5(c), were scanned. The thermal and electronic parameters measured for these points *at steady*

*state* were calculated using our 3D-PTR model and multi-parameter fit method.<sup>4,5</sup> They are shown in Table I. It is seen that, quantitatively, the steady-state PTR lifetime values do not correlate well with the average [Fe] concentrations. Average  $\mu$ -PCD lifetimes, however, show an improved correlation with [Fe]. The steady PTR lifetimes are similar for points a, b, c, but not for d, which has a significantly shorter lifetime value. *It is important, however, to note that, despite differences in the absolute lifetime values between the PTR and  $\mu$ -PCD probes, the details of the overall images of Region A under both PTR (amplitude and phase) and  $\mu$ -PCD probes are very similar to the [Fe] concentration image. This is clearly seen from a comparison among Figs. 5(c), 5(d), and 6, especially 6(a).* It has been shown that PTR amplitude levels in the essentially flat, low-frequency region are approximately proportional to photoexcited carrier lifetimes.<sup>2,5</sup> Therefore, it is clear that the PTR amplitude image is controlled by the Fe concentration via its effect on the local lifetime value at early times after exposure to the laser beam, before the complete onset of low-activation surface annealing effects.<sup>15</sup> The PTR phase, Fig. 6(a), also exhibits similar trends, but no proportionality to the photoexcited carrier lifetime has been established for this signal channel. Calibrating the PTR amplitude image, Fig. 6(a), in terms of quantitative lifetime values, however, is not straightforward either, in view of the results of Table I. During the transient PTR signal evolution, various kinetic, annealing<sup>15</sup> and redistribution Fe processes can take place even at very low fluences changing thermoelectronic properties in *p*-type Si wafers.<sup>12,14,17</sup> The rapid laser-scan conditions that generated Fig. 6 produce minimal disturbance and redistribution of Fe centers and thus offer a more reliable mapping of the original Fe distribution. *In conclusion, fast (nonsteady-state) PTR scanning imaging of Fe-contaminated wafers is desirable as it closely reproduces the Fe concentration distributions.*

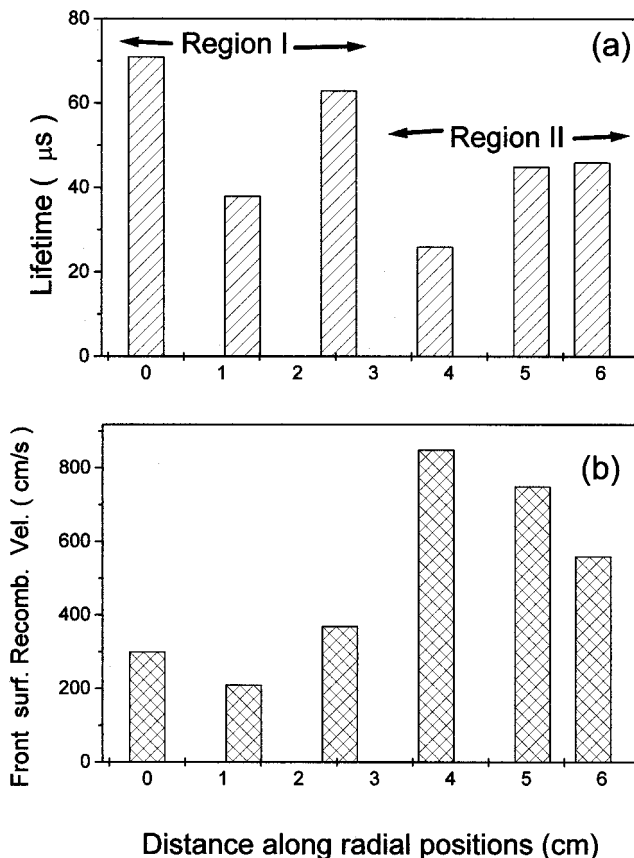


FIG. 4. Histograms of lifetime (a) and front surface recombination velocity (b) for the six points located on sample BK1003. Regions I and II are labeled concentrically away from the wafer center [see Fig. 2(a)].

Figure 7 shows PTR amplitude and phase images of Re-

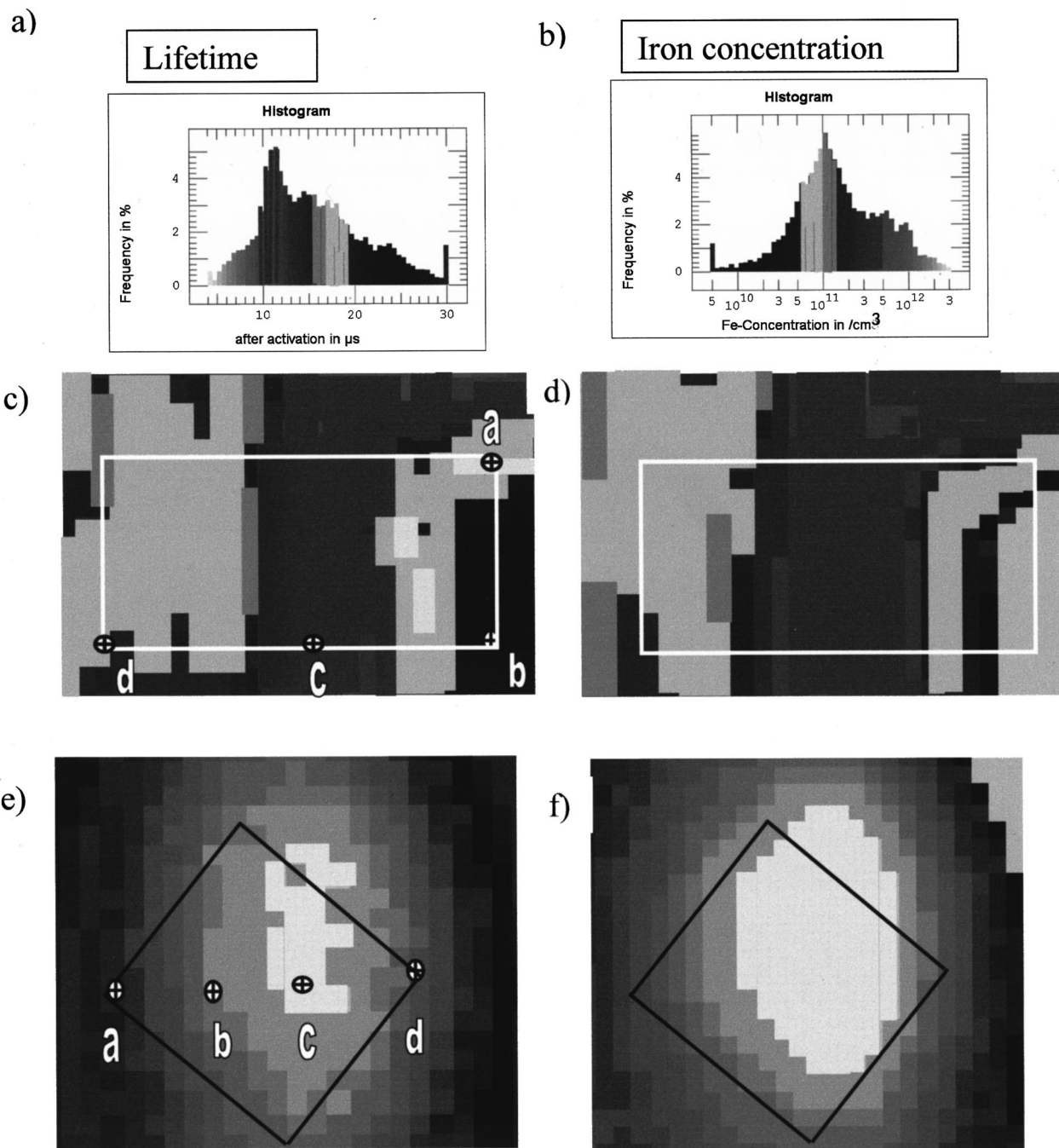


FIG. 5. (a) Histogram of  $\mu$ -PCD lifetime values at 904 nm for wafer BK1003; (b) histogram of  $\mu$ -PCD [Fe] concentration; (c) and (e)  $\mu$ -PCD lifetime maps for Regions A and B, respectively, blown up from Fig. 2(b); (d) and (f)  $\mu$ -PCD [Fe] concentration images of the same regions, blown up from Fig. 2(a).

gion B in sample BK1003, Figs. 2(a) and 5(e). The thermal and electronic parameters found for this region after steady-state conditions are also shown in Table I. Unlike in Region A, across Region B there exists good correlation between  $\mu$ -PCD and PTR lifetimes: points c and d are located in a region which was in contact with the SiC boat, resulting in high [Fe] concentration ( $> 1 \times 10^{12} \text{ cm}^{-3}$ ); also see Fig. 5(f). Accordingly, they exhibit short PTR and  $\mu$ -PDC lifetimes, whereas points a and b, located in a region with relatively lower [Fe] concentration, exhibit higher lifetimes. When compared directly, Figs. 5(e), 5(f), and 7(a) exhibit very similar trends, all of which must be traced to the effects of

[Fe] concentration across the mapped region. The PTR phase, Fig. 7(b) also exhibits similar trends, but no proportionality to the photoexcited carrier lifetime has been established for this signal channel.

Table II shows PTR-derived data from frequency scans at points 1–8 on wafer BK1001 shown in Fig. 2(c). This sample is much more homogeneous than BK1003. According to the  $\mu$ -PCD lifetime data [Fig. 2(d)], the lifetime values in this sample lie in a narrower range (8–10  $\mu\text{s}$ ) than those of wafer BK1003. The PTR results also show that lifetimes do not exhibit drastic variations across the surface of this wafer, including locations close to the flat. There exists ex-

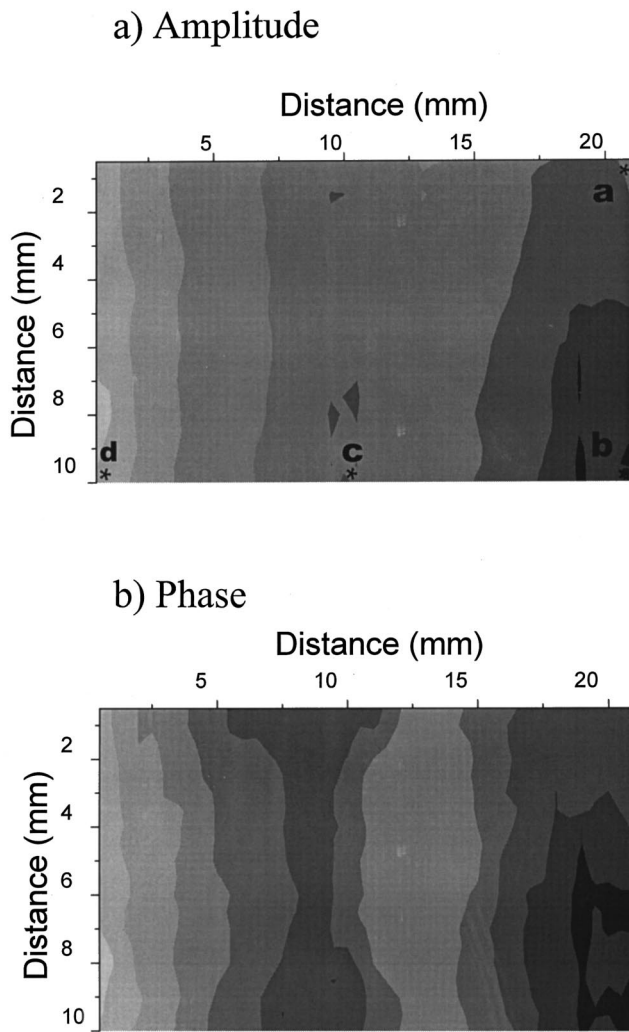
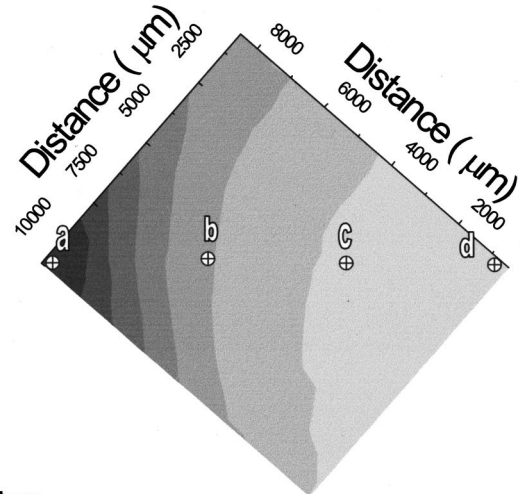


FIG. 6. PTR signal amplitude (a) and phase (b) frequency scans at points (a)–(d) located in Region A, wafer BK1003, Fig. 2(a).

cellent correlation between the  $\mu$ -PCD and PTR lifetime values for this wafer. Region A ( $1 \text{ cm}^2$ ) located at the center of the wafer, Fig. 2(c), was scanned by the  $\mu$ -PCD and the PTR probes. In addition, low-level or no PTR transients were observed. The  $\mu$ -PCD lifetime and [Fe] images inside Region A are very uniform. The PTR amplitude image of the same region is shown in Fig. 8(a). The PTR image shows an enhancement of the small signal gradients from top to bottom, as compared with the  $\mu$ -PCD images of the same area. A plot comparing the  $\mu$ -PCD and PTR lifetimes is shown in Fig. 8(b). This plot shows a linear relationship between the two lifetimes within the constraints of the few data points available. Again, overall, there is excellent agreement between the  $\mu$ -PCD and the PTR lifetime images, even though the absolute steady-state  $\tau_{\text{PTR}}$  values are somewhat greater. As discussed earlier, the difference must be sought in the different photoexcitation wavelengths used with each technique. As in the case of the heavily contaminated wafer BK1003, it is believed that the rapid nonsteady scans of Fig. 8(a) best reflect the lifetime and [Fe] concentration configurations within Region A of wafer BK1001. The excellent correlations between PTR and  $\mu$ -PCD data for this wafer are

(a) PTR Amplitude



(b) PTR Phase

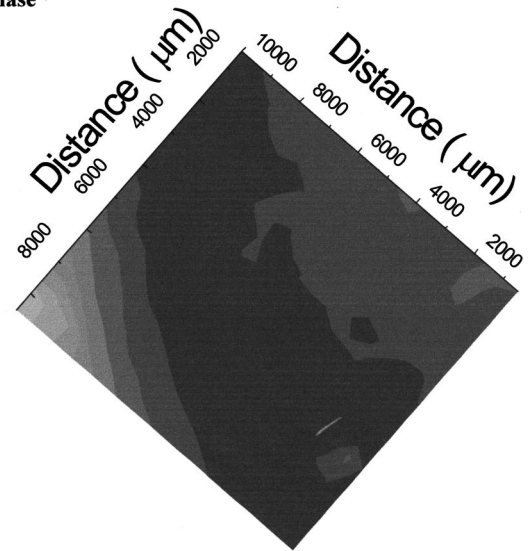


FIG. 7. PTR amplitude (a) and phase (b) images of Region B, wafer BK1003, Fig. 2(a).

attributed to the absence of PTR transients, a strong indicator of higher electronic quality of BK1001 than BK1003.

#### IV. CONCLUSIONS

According to the foregoing results it is clear that 3D PTR metrology is able to determine the thermal and electronic transport properties of Fe-contaminated *p*-Si wafers even at locations where  $\mu$ -PCD probing cannot yield reliable results. The characteristic steady-state PTR photoexcited recombination lifetime measured in both samples was found to follow similar trends to that measured by means of the  $\mu$ -PCD technique, with the PTR values being consistently longer due to differences in excitation wavelengths resulting in different skin depth penetration. The degree of correlation between the calculated PTR and the  $\mu$ -PCD lifetime values was found to vary with the level of Fe contamination of our samples: these values were strongly correlated only for wafer BK1001 which exhibited low [Fe] concentration and weak or no PTR transients upon laser illumination. On the contrary,

TABLE II. Thermal and electronic parameters at eight points across wafer BK1001 (5 in. diameter), Fig. 2(c) determined from the 3D PTR model. The  $\mu$ -PCD lifetime and [Fe] concentration values are also shown. This wafer did not exhibit transient behavior.

Location	Amplitude (mV)	$\alpha$ (cm <sup>2</sup> /s)	$\tau_{\text{PTR}}$ ( $\mu$ s)	$D_n$ (cm <sup>2</sup> /s)	$S_1$ (cm/s)	Average $\tau_{\mu\text{PCD}}$ ( $\mu$ s)	Average [Fe] (cm <sup>-3</sup> )
(1)	11.283	0.25	20	3.60	600	9	$4 \times 10^{11}$
(2)	9.675	0.25	17	3.60	600	7	$4 \times 10^{11}$
(3)	10.002	0.25	17.5	3.60	600	7	$4 \times 10^{11}$
(4)	10.001	0.25	16	3.60	450	6.5	$5 \times 10^{11}$
(5)	9.104	0.25	16	3.60	550	6.5	$4 \times 10^{11}$
(6)	9.331	0.25	16	3.60	550	6.5	$4 \times 10^{11}$
(7)	9.483	0.25	16.5	3.60	550	7	$4 \times 10^{11}$
(8)	9.641	0.25	16.5	3.60	550	7	$4 \times 10^{11}$

much weaker correlation was found for the strongly and non-homogeneously contaminated BK1003 wafer, which exhibited strong PTR signal transients within the near-center Region I, Fig. 4. Transient behavior in highly contaminated areas of sample BK1003, such as Region I, is tentatively associated with FeB dissociation. The increase in the PTR signal as function of the exposure time is possibly related to a concomitant decrease in the local near-surface [Fe] density.

The fast-scanned, nonsteady PTR images from both wafers were very similar to the [Fe] concentration images, as well as to the  $\mu$ -PCD lifetime images. In conclusion, PTR scanning imaging under 515 nm optical excitation produces amplitude and phase images which may be directly related to the near-surface [Fe] concentration distributions and are in good-to-excellent agreement with  $\mu$ -PCD-derived recombination lifetime and [Fe] images. Quantitative PTR measure-

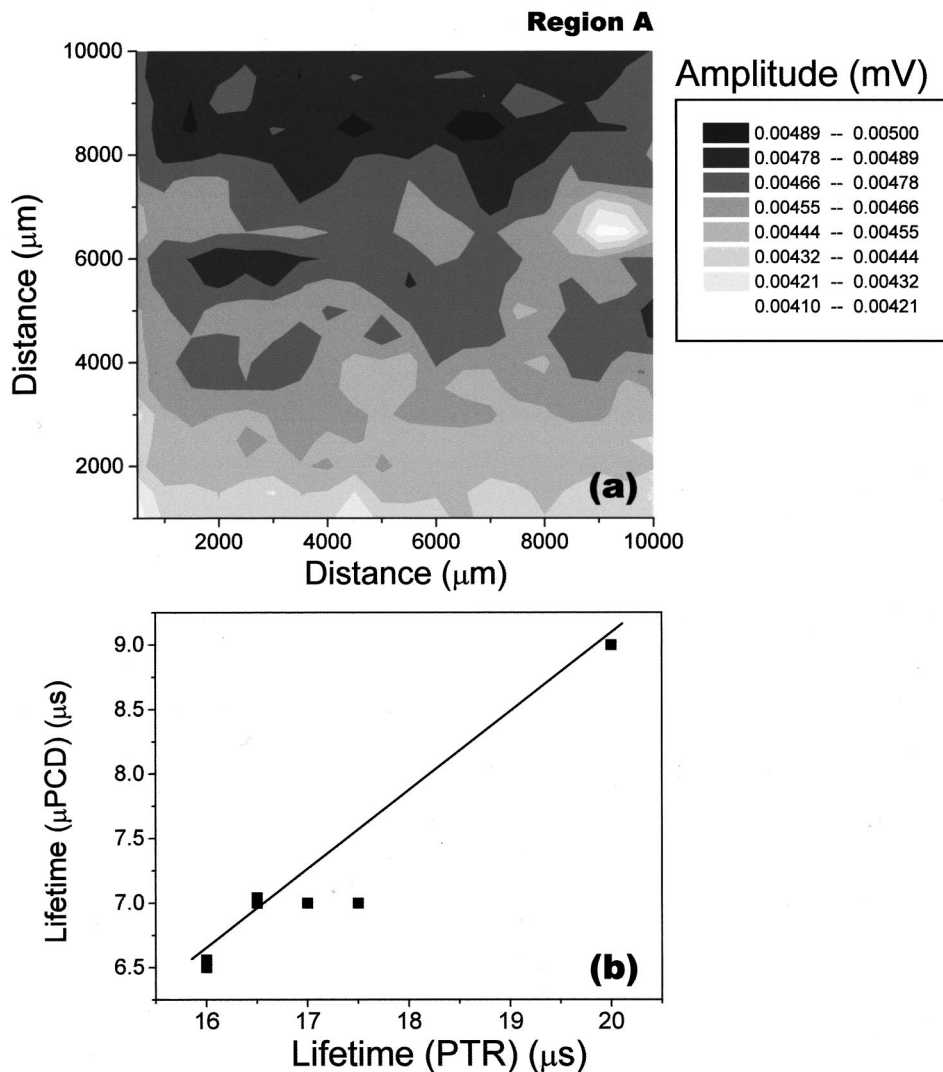


FIG. 8. PTR amplitude image (a), and (b)  $\mu$ -PCD vs PTR lifetimes of Region A, wafer BK1001, Fig. 2(c).

ments of the thermal and electronic transport parameters from steady-state frequency scans are well correlated with local averaged  $\mu$ -PCD lifetime values and  $\mu$ -PCD-derived [Fe] concentrations for lightly and uniformly contaminated *p*-Si; they are not as well correlated with heavily and nonuniformly contaminated samples. For the lightly and uniformly contaminated wafer, PTR scanning imaging was found to be more sensitive to [Fe] concentration and lifetime variations than  $\mu$ -PCD-derived images.

## ACKNOWLEDGMENTS

The authors wish to acknowledge the support of Materials and Manufacturing Ontario (MMO) for an Enabling Grant, and the Natural Sciences and Engineering Research Council of Canada (NSERC) for an Operating Grant. M.E.R. wishes to acknowledge CICATA, México and COLCIENCIAS, Colombia, for their partial support.

<sup>1</sup>*Photoacoustic and Thermal Wave Phenomena in Semiconductors*, edited by A. Mandelis (North-Holland, New York, 1987).

<sup>2</sup>A. Mandelis, *Solid-State Electron.* **42**, 1 (1998).

- <sup>3</sup>A. Salnick, A. Mandelis, H. Ruda, and C. Jean, *J. Appl. Phys.* **82**, 1853 (1997).
- <sup>4</sup>T. Ikari, A. Salnik, and A. Mandelis, *J. Appl. Phys.* **85**, 7392 (1999).
- <sup>5</sup>M. E. Rodríguez, J. A. Garcia, A. Mandelis, G. Pan, and Y. Riopel, *J. Electrochem. Soc.* **147**, 687 (2000).
- <sup>6</sup>A. Rosencwaig, in Ref. 1, Chap. 5, pp. 97–135.
- <sup>7</sup>C. Swiatkowski, in *Proceedings of Recombination Lifetime Measurements in Silicon Workshop (STP1340)*, Santa Clara, CA, 2–3 June 1997, p. 80.
- <sup>8</sup>C. Swiatkowski, A. Sanders, K. D. Buhre, and M. Kunst, *J. Appl. Phys.* **78**, 1763 (1995).
- <sup>9</sup>A. Buczkowski, G. Rozgonyi, F. Shimura, and K. Mishra, *J. Electrochem. Soc.* **140**, 3240 (1993).
- <sup>10</sup>L. Koster, P. Blochl, and L. Fabry, *Jpn. J. Appl. Phys., Part 1* **34**, 932 (1995).
- <sup>11</sup>D. K. Schroder, *Semiconductor Material and Device Characterization* (Wiley, New York, 1998).
- <sup>12</sup>G. Zoth and W. Bergholz, *J. Appl. Phys.* **67**, 6764 (1990).
- <sup>13</sup>Y. Kitagawara, T. Yoshida, T. Hamaguchi, and T. Takenaka, *J. Electrochem. Soc.* **142**, 3505 (1995).
- <sup>14</sup>M. Miyasaki, S. Miyasaki, T. Kitamura, T. Aoki, Y. Nakashima, M. Hourai, and T. Shigamatsu, *Jpn. J. Appl. Phys., Part 1* **34**, 409 (1995).
- <sup>15</sup>M. E. Rodríguez, A. Mandelis, J. A. Garcia, Y. Riopel, and J. Claude, *Appl. Phys. Lett.* **74**, 2429 (1999).
- <sup>16</sup>A. Dargys and J. Kundrotas, *Handbook on Physical Properties of Ge, Si, GaAs and InP* (Vilnius, Lithuania, 1994).
- <sup>17</sup>A. Salnik, A. Mandelis, and C. Jean, *Appl. Phys. Lett.* **69**, 17 (1996).